VALIDATION OF CIRA'S ROTORCRAFT AERODYNAMIC MODELLING SYSTEM WITH DNW EXPERIMENTAL DATA

A. Visingardi, A. D'Alascio, A. Pagano, and P. Renzoni
CIRA, Italian Aerospace Research Center
Capua, Italy

Abstract

The unsteady panel code, RAMSYS (**R**otorcraft **A**erodynamic **M**odelling **SYS**tem), has been developed for the analysis of multi-body configurations in arbitrary flight.

Free-wake modelling is combined with an interactional methodology for the study of the interactional aerodynamics about complex configurations. A variable time step strategy has been adopted to allow large time steps during the convergence process and small time steps in regions of the rotor disk that are particularly interactional. In order to correct the classical *steady* Kutta condition an iterative procedure is implemented in RAMSYS that imposes a continuous pressure across the trailing edge.

The validation of the code is done on test data for two model rotors tested in the DNW in the framework of the European cooperative research projects HELINOISE and HELISHAPE. Particular attention is payed to hover and low-speed forward flight conditions where there are significant interactions between the blades and the wake. Good agreement with the test data is obtained for a hovering rotor. The BVI phenomenology arising on a low-speed level flight rotor is correctly modelled. Good results are also observed for an isolated rotor in a low-speed 12° climb. The interaction with the fuselage gives a fair agreement with some discrepancies appearing in the third quadrant of the rotor disk.

List of Symbols

c	Blade chord
C_n	Section normal force/$(0.5\rho_\infty V^2 c)$
C_p	Pressure coefficient
C_T	Rotor thrust coefficient
M_H	Hover tip Mach number
n	Time iteration index
$\mathbf{n}$	Normal vector
r	Blade radial coordinate
R	Rotor radius
t	Time
$\mathbf{v}$	Velocity vector
$\mathbf{V}$	Roto-translational velocity vector
V	Local blade velocity
$\mathbf{x}$	Position vector
$\mathbf{x}_*$	Control point position vector
μ	Advance ratio
ρ_∞	Free stream density
ϱ	Distance $\parallel \mathbf{x} - \mathbf{x}_* \parallel$
ϕ	Velocity potential
ψ	Normalwash
Ψ	Blade azimuthal position
$\Delta\phi$	Velocity potential jump

Introduction

The prediction of the flow field about rotorcraft is still today one of the most challenging problems to the helicopter research community. The multiple interactions among the various components and the presence of transonic and viscous dominated flow regions make the use of a single prediction code not yet practical. Even though great strides have been made in computational fluid dynamics (CFD), with emphasis on Navier-Stokes methodologies (Ref 1), significant improvements both in algorithms and in computers are required before rotorcraft CFD methods are used routinely by the helicopter industry.

A more traditional and practical approach to rotorcraft aerodynamics is to link/couple low-order formulations for different components (*i.e.* blade, fuselage) and use more complex formulations when greater accuracy is required. CIRA is developing a prediction code for complex rotorcraft configurations

based on linear potential flow theory. The RAMSYS code (**R**otorcraft **A**erodynamic **M**odelling **SYS**tem) is based on Morino's boundary integral formulation for bodies in arbitrary rigid-body motion in subsonic compressible flow (Refs 2,3). Preliminary validation of the formulation has shown promising results in terms of correctly modelling flow field characteristics (Ref 4) and blade loading (Ref 5).

The aim of this paper is to validate the RAMSYS code on test data for two model rotors tested in the DNW in the framework of the European cooperative research projects HELINOISE and HELISHAPE (Refs 6,7). Particular attention will be payed to hover and low-speed forward flight conditions where there are significant interactions between the blades and the wake.

Description of RAMSYS

RAMSYS is an unsteady panel code for multi-body configurations based on Morino's boundary integral formulation. Although the formulation is valid for compressible flows, this paper focuses on the incompressible version of RAMSYS.

For incompressible flows the formulation consists in the solution of Laplace's equation written in terms of the velocity potential ϕ

$$\nabla^2\phi = 0 \qquad \forall \mathbf{x} \notin \mathcal{S}(t) \qquad (1)$$

such that $\mathbf{v} = \nabla\phi$. $\mathcal{S}(\tau)$ is a surface outside of which the flow is potential and consists of a surface S_B surrounding the body geometry and a surface S_W surrounding the wake geometry.

The boundary condition at infinity is that $\phi = 0$. The surface of the body is assumed to be impermeable hence $\frac{\partial\phi}{\partial n} = \mathbf{v}_B \cdot \mathbf{n}$ where $\mathbf{v}_B$ is the velocity of a point on the body. The wake is a surface of discontinuity which is not penetrated by the fluid and across which there is no pressure jump. The second wake condition implies that $\Delta\phi$ remains constant following a wake point $\mathbf{x}_W$, and equal to the value it had when $\mathbf{x}_W$ left the trailing edge.

The value of $\Delta\phi$ at the trailing edge is obtained by using the Kutta-Joukowski hypothesis that no vortex filament exists at the trailing edge; this implies that the value of $\Delta\phi$ on the wake and the value of $\Delta\phi$ on the body are equal at the trailing edge.

The application of Green's function method to Eq.(1), yields the following boundary-integral-representation for the velocity potential ϕ

$$E(\mathbf{x}_*)\phi(\mathbf{x}_*, t_*) = I_B + I_W \qquad (2)$$

with

$$I_B = \oiint_S \left[\left(-\frac{1}{4\pi\varrho}\right)\frac{\partial\phi}{\partial n} - \phi\frac{\partial}{\partial n}\left(-\frac{1}{4\pi\varrho}\right)\right] dS$$

and

$$I_W = -\iint_{S_W} \Delta\phi \frac{\partial}{\partial n}\left(-\frac{1}{4\pi\varrho}\right) dS$$

representing respectively the contribution of the body and the wake. $E(\mathbf{x}_*)$ is a domain function defined as zero inside $\mathcal{S}$ and unity elsewhere.

The helicopter geometry and the wake are respectively discretised by M and N hyperboloidal quadrilateral panels on which the unknown velocity potential, the normalwash and the velocity potential jump are constant (zeroth-order formulation). Using the collocation method and setting the collocation points at the centroids of each element on the body geometry, the integral equation, Eq.(2), is replaced by an algebraic linear system of equations for the velocity potential ϕ:

$$E_k\phi_k(t) = \sum_{m=1}^{M} B_{km}\psi_m(t) + \sum_{m=1}^{M} C_{km}\phi_m(t) + \sum_{n=1}^{N} F_{kn}\Delta\phi_m(t) \qquad (3)$$

where B, C, and F are respectively the body source, body doublet, and wake doublet influence coefficients. A Conjugate Gradient Method (GMRES solver) is applied for the numerical solution of the problem.

A particular feature of the code is the implementation of the Kutta condition. The classical *steady* Kutta condition, implemented in terms of the potential jump at the trailing edge, often leads to large pressure jumps across the trailing edge of rotor blades. Such behaviour is more relevant at the root and tip of the blades where the 3D phenomena are predominant.

In order to impose a continuous pressure across the trailing edge an iterative procedure (Ref 8) has been implemented in RAMSYS with which for each trailing-edge wake panel the pressure jump, computed by applying Bernoulli's equation for unsteady flows, has been explicitly set equal to zero. In this way a number of additional nonlinear equations are coupled with the system of equations, Eq.(2):

$$\Delta\left[\frac{\partial\phi^{n+1}}{\partial t} + \mathbf{V}\cdot\nabla\phi^{n+1} + \frac{1}{2}\nabla\phi^{n}\cdot\nabla\phi^{n+1}\right] = 0 \qquad (4)$$

These equations give a correction to the RHS of the system, Eq.(2), which in turns gives a better approximation for the gradient of the velocity potential that appears in Eq.(4).

A time-marching free-wake model is implemented in RAMSYS. Wake panels are released at each time step from the trailing edge as the lifting body moves through an inertial frame of reference. Therefore, the shape of the wake is a consequence of the local induced velocities which are evaluated from Eq.(2) as:

$$\begin{aligned} \mathbf{v}_i &= \oiint_S \left[\left(-\frac{\varrho}{4\pi\varrho^3}\right)\frac{\partial\phi}{\partial n} - \phi\frac{\partial}{\partial n}\left(-\frac{\varrho}{4\pi\varrho^3}\right)\right] dS \\ &- \iint_{S_W} \Delta\phi\frac{\partial}{\partial n}\left(-\frac{\varrho}{4\pi\varrho^3}\right) dS \end{aligned} \tag{5}$$

A Rankine vortex-core model and the Baron-Boffadossi (Ref 9) vortex-core model are available to stabilize the wake. Since the wake is *cut* a certain distance from the rotor, the remaining *far wake* is represented by a disk of sinks and doublets.

The simple use of free-wake modelling can be successfully employed for flight conditions where the interactions between the wake and the rotor are relatively mild. However, for strong interactions in which the wake penetrates the body surface this approach leads to unphysical solutions. The present version of RAMSYS implements the method proposed by Clark and Maskew (Ref 10) for body/wake interactions. It consists in cancelling the strength of the wake panels impacted (penetrated) by the surface. This leaves a raw edge in the wake sheet which subsequently deflects under its own influence. The surface panels pick up the jump in singularity strength associated with the raw edge and contribute to the local distortion. Although the model doesn't represent exactly the physics of the problem, it nevertheless provides a working model of the phenomenon. A special treatment of the raw-edge wake region is required in order to prevent the excessive overshoots typical of potential-based methods.

The modelling of strongly interactional phenomena such as BVI requires very fine temporal discretisations (less than 1°). RAMSYS employs a variable time step strategy within each single rotor revolution thus allowing for large time steps during the convergence process and for small time steps in regions of the rotor disk that are particularly interactional.

Test Cases for Validation

Two recent test campaigns in the DNW, carried out in the framework of the HELINOISE and HELISHAPE projects, have provided extensive pressure data on model rotors in different flight conditions. Data from these two tests have been used to validate RAMSYS. The principal characteristics of the model rotors are:

- HELINOISE - BO 105 Model Rotor
  This four-bladed hingeless rotor has linearly twisted blades of rectangular planform, an aspect ratio of 16.52 and non symmetrical modified NACA 23012 airfoils.
- HELISHAPE - ONERA/ECF 7A Model Rotor
  This four-bladed articulated rotor has linearly twisted blades of rectangular planform, an aspect ratio of 15 and non symmetrical OA2xx airfoils with varying thickness from 13 to 9 percent.

Three different test cases have been chosen to assess the ability of RAMSYS in predicting strongly interactional flow fields:

- HELISHAPE DPt 59
  ↪ Hover @ nominal tip speed
- HELINOISE DPt 344
  ↪ Low-speed level flight
- HELINOISE Dpt 508
  ↪ Low-speed 12°-climb

Results and Discussion

Two different spatial discretizations have been adopted in RAMSYS to model the *main* blade and the *secondary* blades of the two rotors studied. The surface panelling of the main blade consists of 60 panels around the airfoil and 10 panels in the spanwise direction whereas the secondary blades have been discretised by 20 panels around the airfoil and 10 panels along the blade span. Smaller panels have been used toward the blade tip and at the leading edge of the airfoils.

The temporal discretisation is adapted to the characteristics of the test case: steady or unsteady, strongly interactional or not. The structure of the code permits the refinement of the temporal discretisation in regions where strongly interactional phenomena may be expected.

A prescribed wake modelling is used to reach a periodic behaviour of the thrust coefficient after which a free wake computation is performed for at least two

rotor revolutions. The correction of the Kutta condition is applied only at the last rotor revolution.

HELISHAPE DPt 59: This test case refers to a hovering rotor ($\mu = 0.$) at $C_T = 0.00436$ and $M_H = 0.617$. Eight rotor revolutions have been performed with an azimuthal step of 45° for the first six revolutions and 30° for the last two. The complex geometries of the airfoils employed has required small panels both at the leading and trailing edge of the blade.

Fig 1 compares the measured and the predicted tip vortex trajectories. The vertical descent of the tip vortex (Fig 1a) is predicted well. The predicted radial contraction (Fig 1b) is in reasonable agreement with the measurements and the observed increase in the contraction near 220° is captured.

The spanwise blade loading is shown in Fig 2a. The agreement with the test data is good. The comparison between the numerical and the experimental pressure distribution along the blade confirms the good agreement (Figs 2b-2c). An overestimation of the expansion on the upper side of the blade, due to compressibility effects, is observed toward the tip.

HELINOISE DPt 344: This test case deals with a low-speed level flight ($\mu = 0.15$) in the presence of mild BVI effects at $C_T = 0.00446$ and $M_H = 0.644$. Four rotor revolutions have been performed, the first two with an azimuthal step of 30° and the other two with a variable azimuthal step ranging from 5°, where BVI is present, to 15°.

The normal force time history (C_n normal to the local chord) is shown in Fig 3 at the $r/R = 0.87$ and $r/R = 0.97$ stations. The presence of BVI is revealed by two irregular peaks in the test data respectively around $\Psi = 90°$ and $\Psi = 270°$. The comparison between the numerical and experimental results is good since BVI effects are correctly localised by RAMSYS. The sharp BVI peaks in the numerical results, which are however a characteristic of a potential modelling of the problem, might be reduced by furtherly decreasing the azimuthal step.

A critical test for the pressure results is the prediction of its time history. As the BVI phenomena are most severe near the blade leading edge, the variation of pressure on blade surface over azimuth at two selected chord station and two radial stations are compared with experimental results in Fig 4.

As for the normal force time history, the phenomenology is qualitatevely well captured by the theory. A comparison of the results at the two chord stations highlights the effect of BVI which is stronger near the leading edge.

A quantitative discrepancy with the test results is here believed to be caused not only by viscosity but also by the elastic torsional deformation of the blade, not considered in this analysis, which can significatively change the blade twist distribution.

Fig 5 illustrates the chordwise pressure distribution at different azimuthal positions at the station $r/R = 0.87$. The agreement is generally satisfactory. Small discrepancies can be observed on the upper side of the blade in the region of the advancing blade which may be attributed to compressibility effects. A downward shift with respect to the test data is generally present on the lower side of the blade. The reason for this discrepancy is at the present not known.

HELINOISE Dpt. 508: This test case studies a low-speed 12°-climb ($\mu = 0.15$) at $C_T = 0.00454$ and $M_H = 0.645$. The analysis has been performed on the isolated rotor as well as on the rotor/fuselage configuration in order to assess the ability of the code in dealing with the interaction between the rotor wake and the fuselage. Four rotor revolutions have been performed, the first three with an azimuthal step of 30° and the last one with an azimuthal step of 15°. The Modular Wind tunnel Model (MWM), representing a BO-105 like model fuselage, has been discretised by 1488 panels.

Fig 6 shows the wake that develops around the isolated rotor (Fig 6a) and the rotor/fuselage configuration (Fig 6b). A view of the configurations showing only the wake of the main blade (Fig 6c) is provided for clarity. A cross-sectional view is given in Fig 7 showing the effect of the fuselage on the wake.

The C_n time history is shown in Fig 8 at the $r/R = 0.87$ and $r/R = 0.97$ stations. The agreement with the experimental results is very good as far the isolated rotor is concerned. The behaviour of the test data is resembled very closely by the theory which is only shifted more upward than the experiment. The presence of the fuselage determines an increase of the normal force with respect to the isolated rotor in the rearward part of the rotor disk that can be explained by a kind of blockage effect that the fuselage exerts on the wake. In the forward region of the rotor disk, the fuselage tends to reduce the normal force as if a downwash were introduced by its presence.

A global overestimation with respect to the test data is instead observed for both isolated rotor and rotor/fuselage configurations, with the only exception of the third quadrant of the rotor disk at the more inboard radial station where the test data are in a better agreement with the computed results for the isolated rotor.

Fig 9 illustrates the chordwise pressure distribution at different azimuthal positions at the station $r/R = 0.87$. The agreement is generally satisfactory with the test data. No difference is observed on the lower surface of the blade between the isolated rotor and the rotor/fuselage configuration whereas different behaviours on the upper surface of the blade can be observed between the two configurations by passing from the rearward part of the rotor to the upward part of it.

It is noteworthy to point out that the two configurations are run at constant C_T which is obtained by varying the shaft angle while maintaining constant the control angles given by the experiment. It is likely that this procedure is the cause of some of the discrepancies. Work is ongoing in introducing a trim loop in RAMSYS.

Conclusions

A validation of the RAMSYS code has been done on test data for two model rotors tested in DNW. The test cases have been chosen at three low-speed operating conditions posing different levels of difficulty for the numerical simulation.

The hover test case has shown the ability of the code in predicting the wake development through free-wake modelling. A low-speed level flight test case has been studied in order to investigate the ability of RAMSYS in capturing the complex flowfield around the blades in presence of mild BVI effects. The agreement between the experiment and the theory has been very satisfactory from a quantitative point of view. The overestimation observed in the numerical results have been explained by the inviscid nature of the code and by the existence of aeroelastic effects which are not modelled by RAMSYS. A rotor/fuselage configuration in low-speed 12° climb has been finally studied in order to test the interactional strategy employed in the code. The results have been compared with the test data and with the numerical results of the isolated rotor in the same test conditions. A stronger influence of the fuselage is observed in the more inboard radial station where the fuselage is closer to the rotor. Apart from the usual overestimating behaviour of the code, some discrepancies have been observed in the third quadrant of the rotor disk which require further investigation.

The ability of RAMSYS in simulating multi-body configurations in arbitrary flight offers the perspective of its use to provide accurate results for both aerodynamic and aeroacoustic analyses. A further step ahead will be constituted by the implementation of the subsonic compressible formulation in the code.

Acknowledgements

This work was partially supported by the European Union under the Brite-EuRam Contract No. AER2-CT92-0047 (HELISHAPE project).

References

1. Landgrebe, A.J., "New Directions in Rotorcraft Research in the US," 75th AGARD Fluid Dynamics Panel Symposium on Aerodynamics and Aeroacoustics of Rotorcraft, Berlin, Germany, Oct. 1994.

2. Gennaretti, M., Macina, O., and Morino, L., "A New Integral Equation for Potential Compressible Aerodynamics of Rotors in Forward Flight," Proceedings of the International Specialist's Meeting on Rotorcraft Basic Research, Atlanta, U.S.A., March 1991.

3. Morino, L., Gennaretti, M., and Petrocchi, P., "A General Theory of Potential Aerodynamics with Applications to Helicopter Rotor-Fuselage Interaction," Symposium of the International Association for Boundary Element Methods, Kyoto, Japan, Oct. 1991.

4. Renzoni, P., Visingardi, A., and Pagano, A., "Validation of a Boundary Integral Formulation for the Aerodynamic Analysis of Rotors in Forward Flight," Proceedings of the Eighteenth European Rotorcraft Forum, Avignon, France, Sept. 1992.

5. Visingardi, A., "A Boundary Integral Formulation for the Aerodynamic Analysis of Parallel Blade-Vortex Interactions over Aerofoils," Proceedings of the Nineteenth European Rotorcraft Forum, Cernobbio, Italy, Sept. 1993.

6. Splettstösser, W.R., Niesl, G., Cenedese, F., Nitti, F., and Papanikas, D.G., "Experimental Results of the European HELINOISE Aeroacoustic Rotor Test in the DNW," Proceedings of the Nineteenth European Rotorcraft Forum, Cernobbio, Italy, Sept. 1993.

7. Klöppel, V., "Rotorcraft Aerodynamics and Aeroacoustics (HELISHAPE)," Technical Annex, Contract No. AER2-CT92-0047 (DG 12 WSME), Aug. 1993.

8. Kinnas, S.A. and Hsin, C.-Y., "Boundary Element Method for the Analysis of the Unsteady Flow Around Extreme Propeller Geometries," *AIAA Journal*, Vol. 30, No. 3, 1992, pp. 688-696.

9. Baron, A. and Boffadossi, M., "Numerical Simulation of Unsteady Rotor Wakes," Proceedings of the Seventeenth European Rotorcraft Forum, Berlin, Germany, Sept. 1991.

10. Clark, D.R. and Maskew, B., "Calculation of Unsteady Rotor Blade Loads and Blade/Fuselage Interference", II International Conference on Rotorcraft Basic Research, College Park, U.S.A., Feb. 1988.

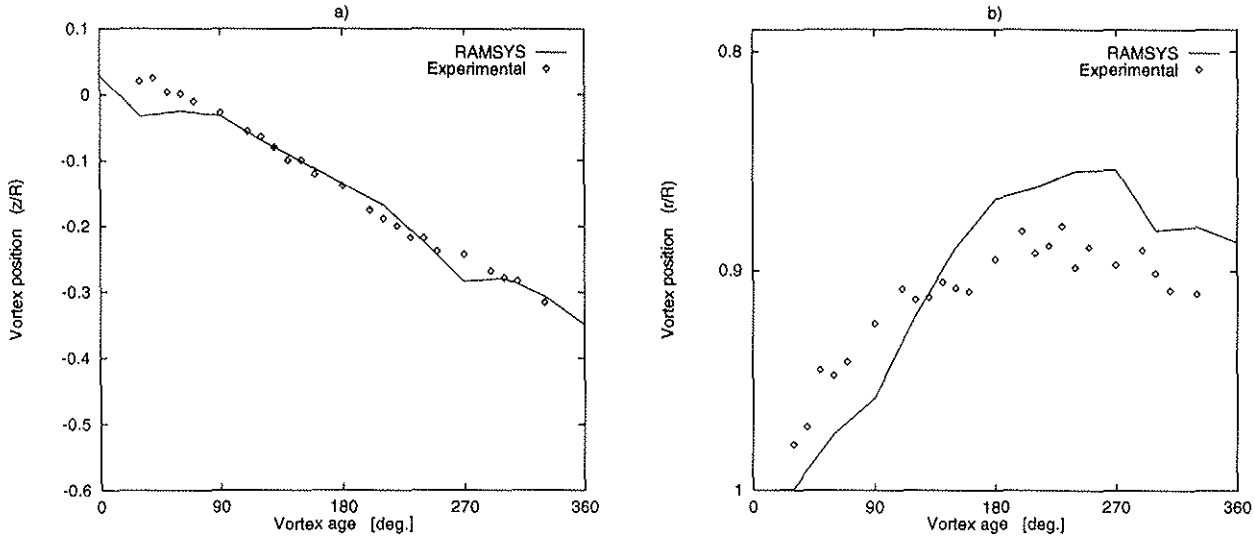

Fig 1 : Tip vortex trajectories in hover a) vertical descent b) radial contraction.

(DPt 59 : Hover @ nominal tip speed, $C_T = 0.00436$, $M_H = 0.617$)

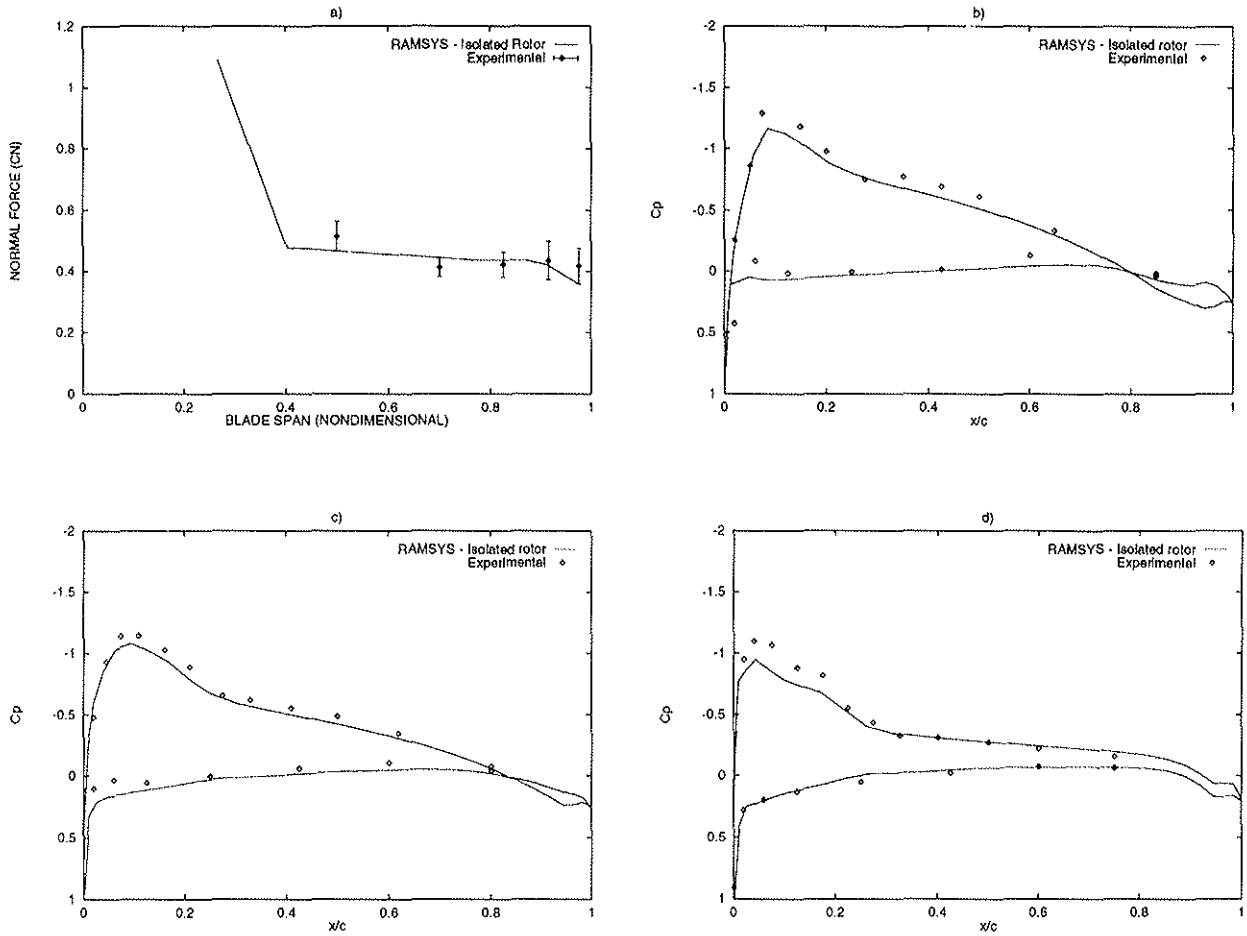

Fig 2 : a) Normal force along blade span and b)-d) pressure distributions at three radial stations $r/R = 0.7, 0.815, 0.975$

(DPt 59 : Hover @ nominal tip speed, $C_T = 0.00436$, $M_H = 0.617$)

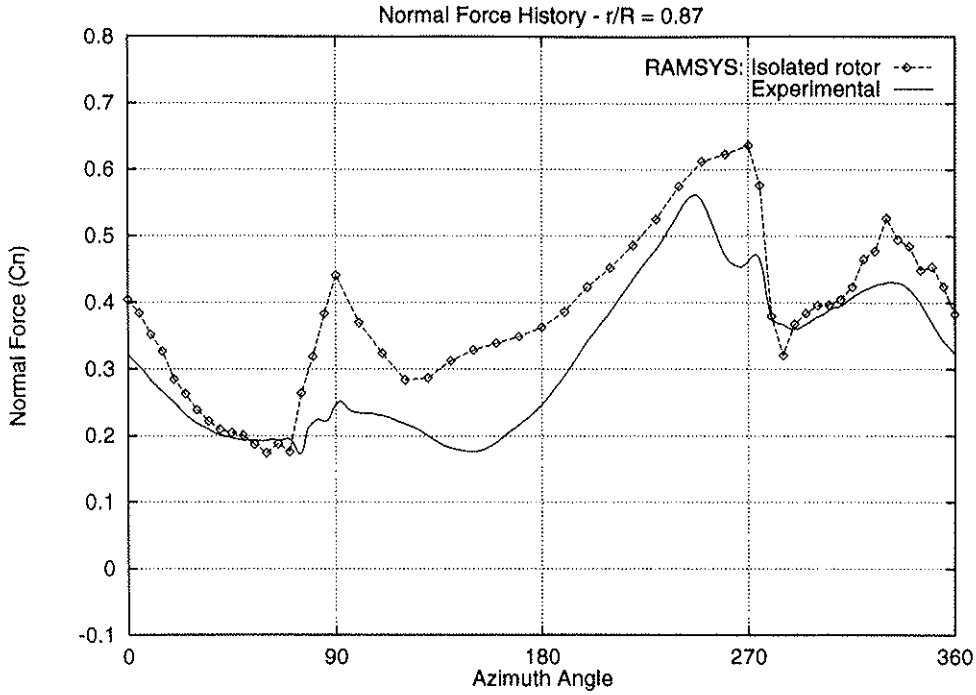

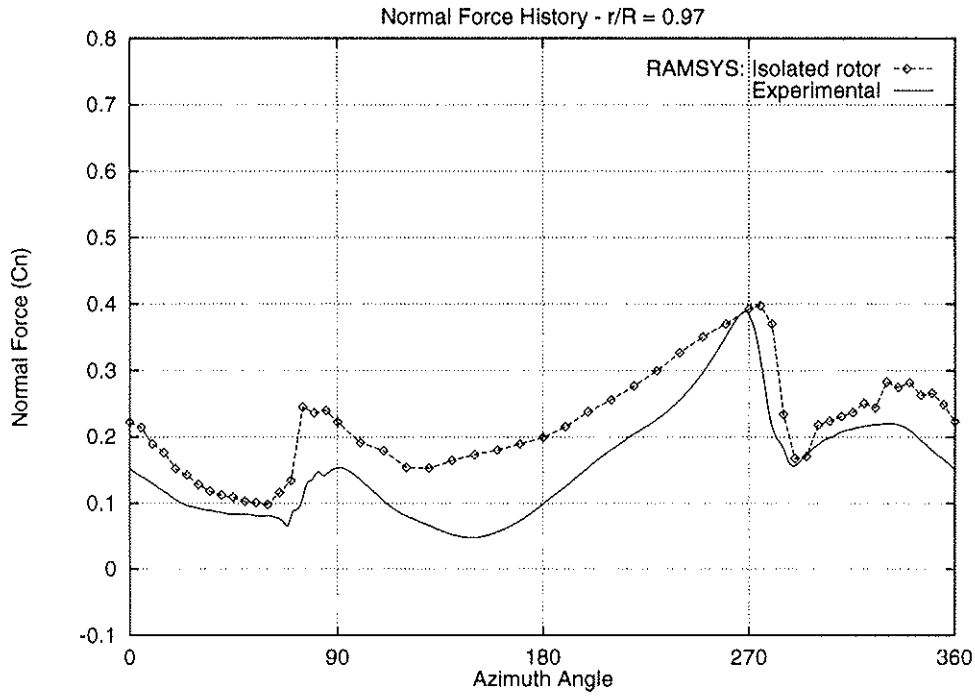

Fig 3 : Normal force time history at two radial stations ($r/R = 0.87, 0.97$).

(DPt 344 : Low-speed level flight, $\mu = 0.15, C_T = 0.00446, M_H = 0.644$)

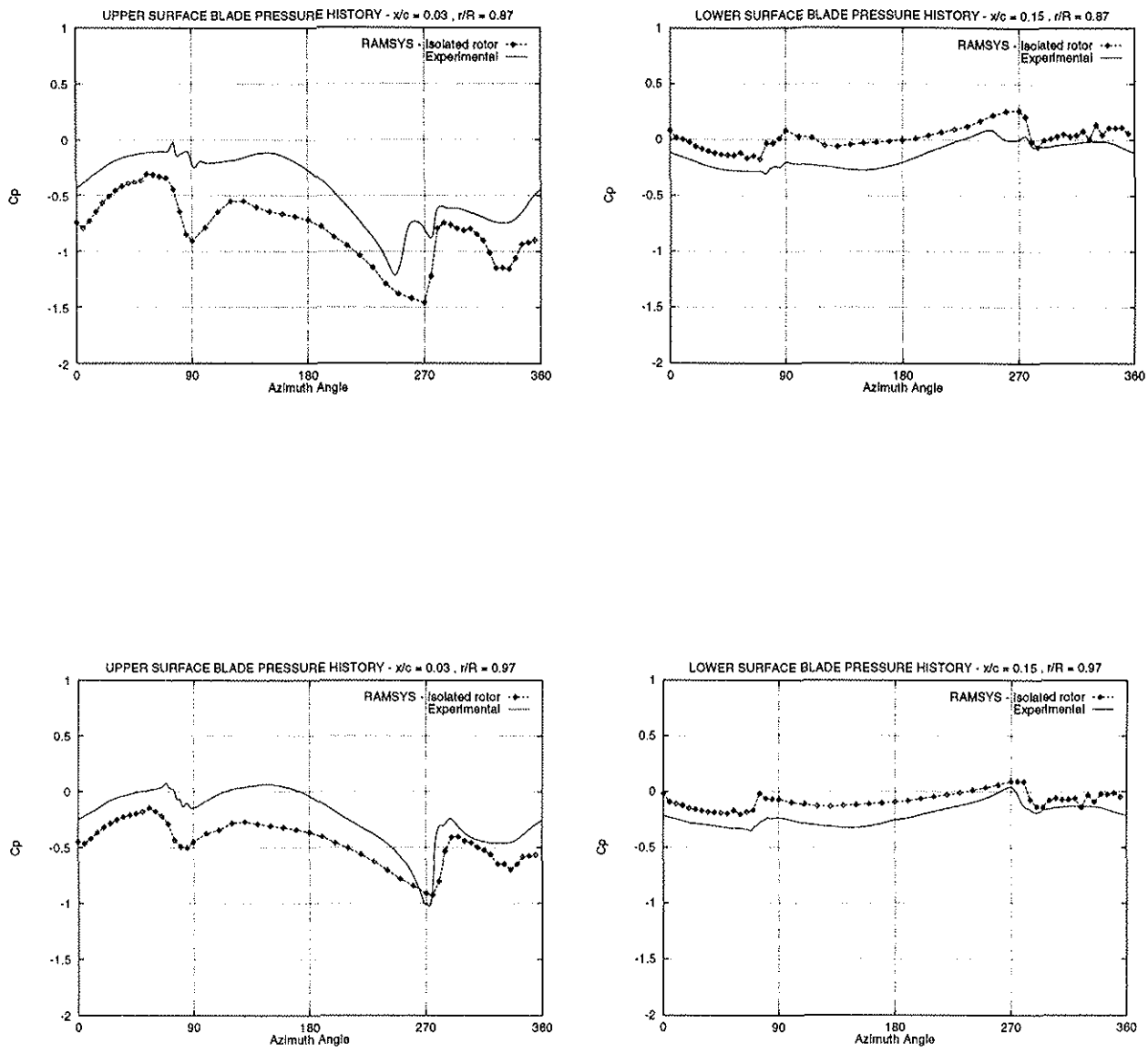

Fig 4 : Pressure time history at two chordwise positions ($x/c = 0.03$ upper, $x/c = 0.15$ lower). on two radial sections ($r/R = 0.87, 0.97$)

(DPt 344 : Low-speed level flight, $\mu = 0.15, C_T = 0.00446, M_H = 0.644$)

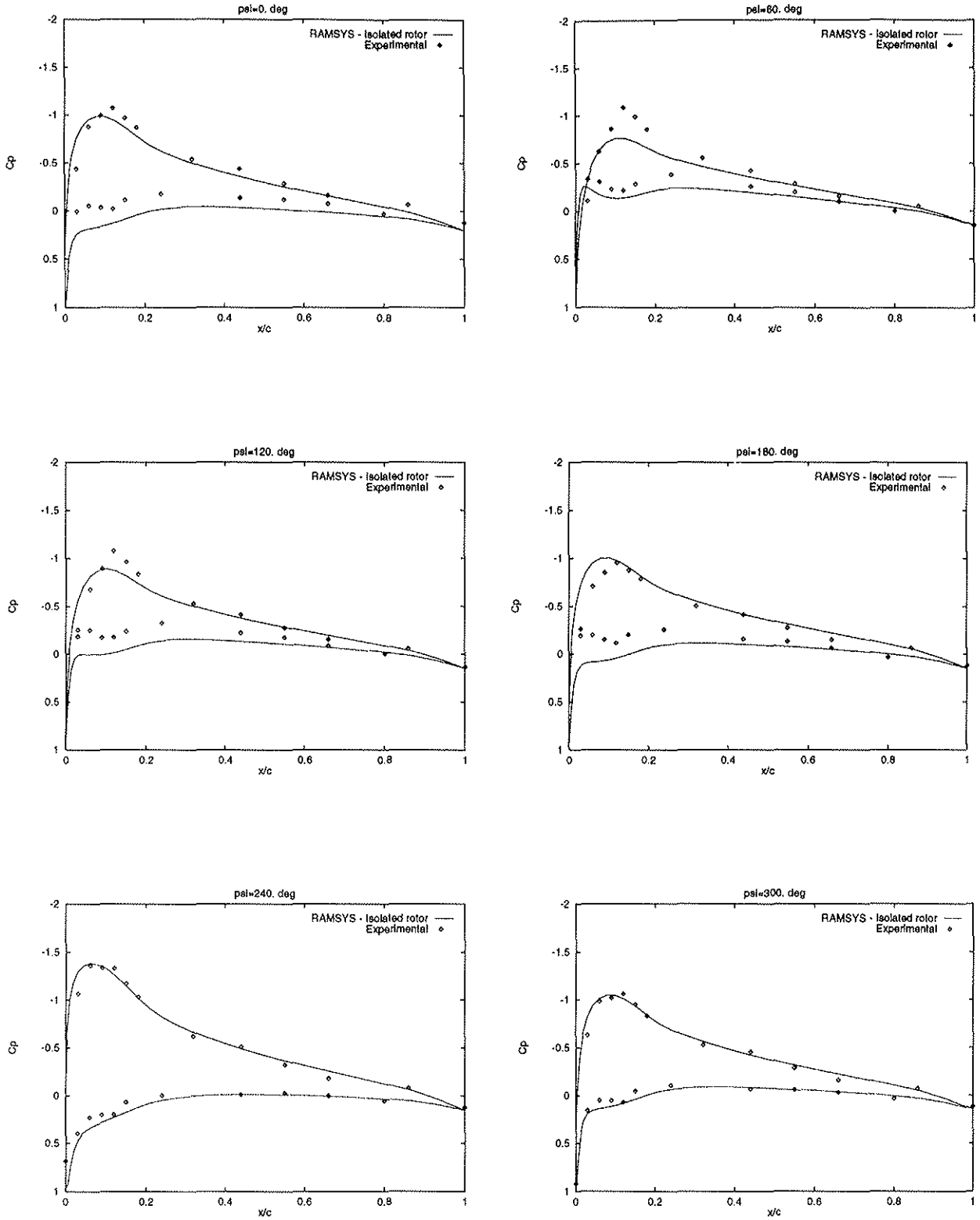

Fig 5 : Chordwise pressure distribution at a single radial station ($r/R = 0.87$) for six azimuthal positions ($\Psi = 0° - 300°$).

(DPt 344 : Low-speed level flight, $\mu = 0.15, C_T = 0.00446, M_H = 0.644$)

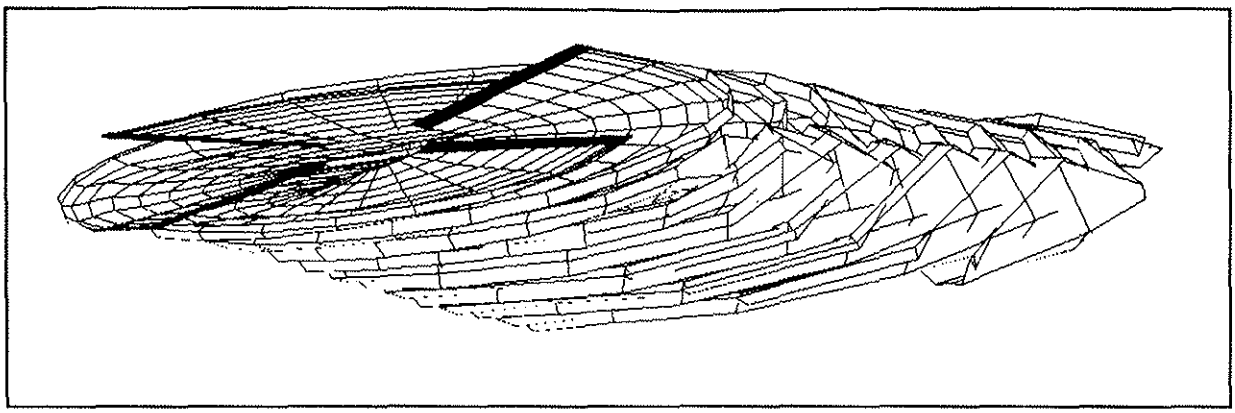

a)

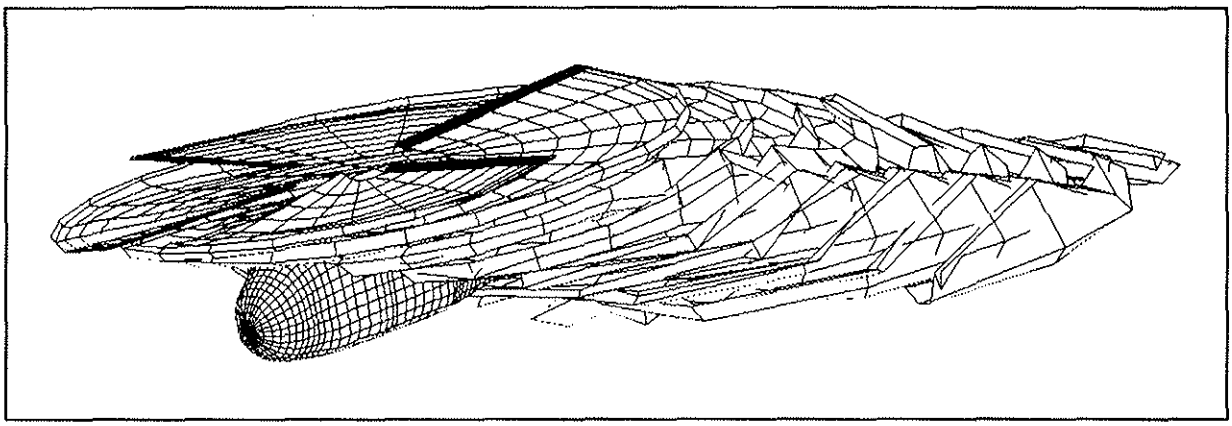

b)

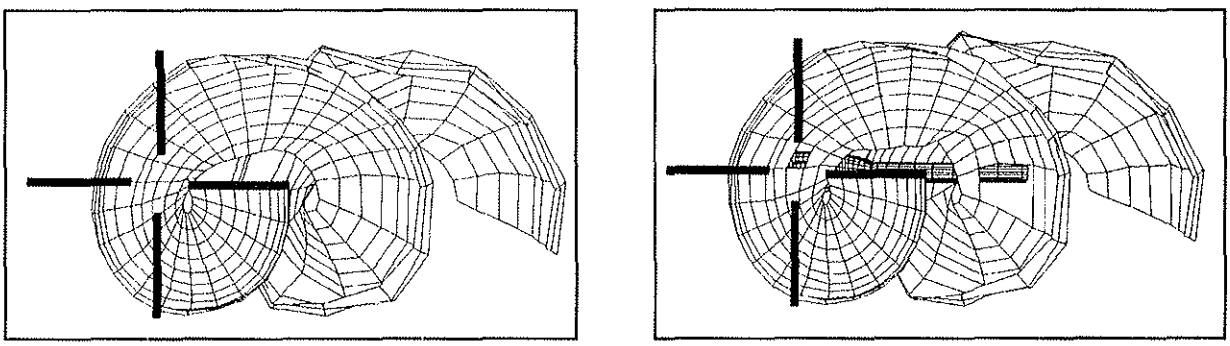

c)

Fig 6 : Development of the free wake about a) the isolated rotor and b) the rotor fuselage configuration. The wake from the main blade is shown in isolation for clarity in c). (DPt 508 : Low-speed 12°-climb, $\mu = 0.15, C_T = 0.00454, M_H = 0.645$)

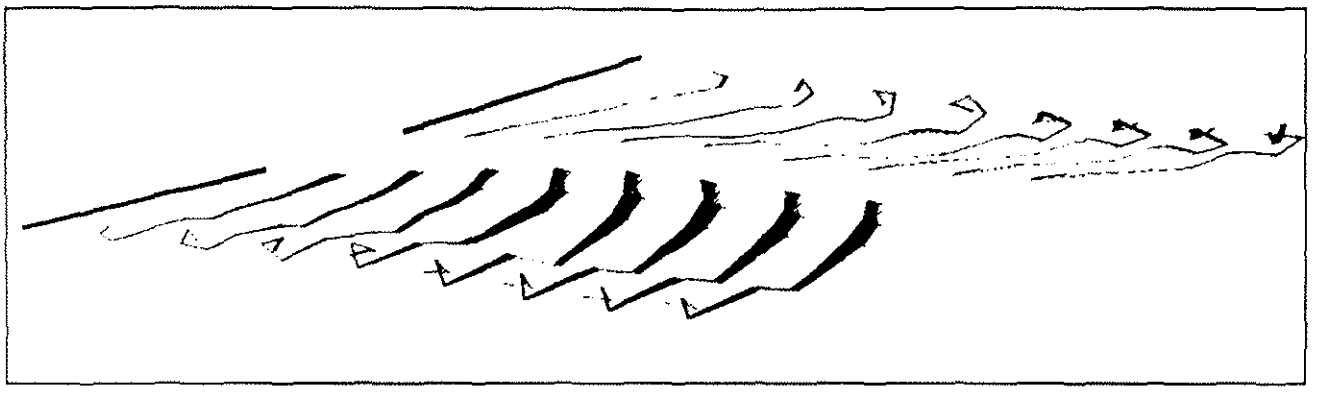

a)

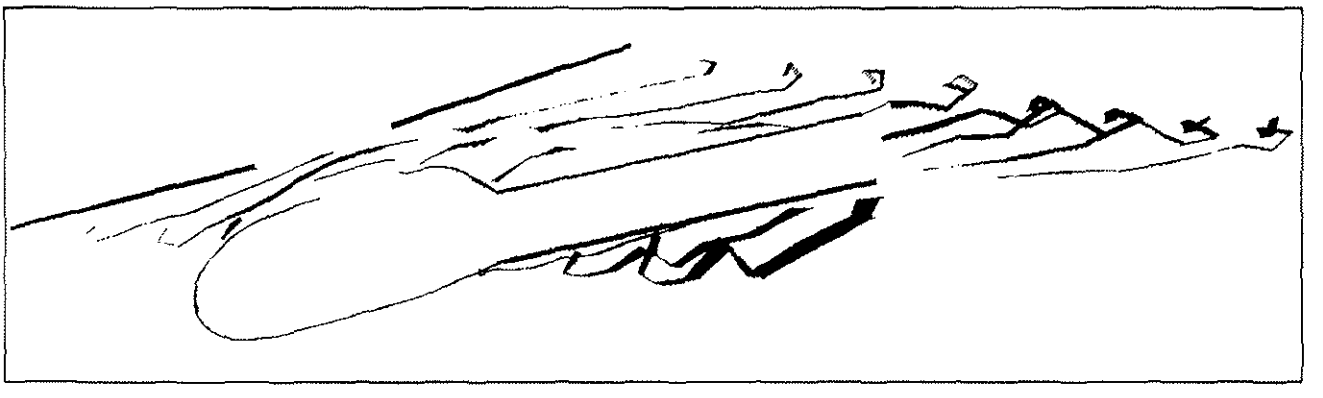

b)

Fig 7 : Cross-sectional view of the wake generated by a) the isolated rotor configuration and b) the rotor/fuselage configuration.
(DPt 508 : Low-speed 12°-climb. $\mu = 0.15$. $C_T = 0.00454$. $M_H = 0.645$)

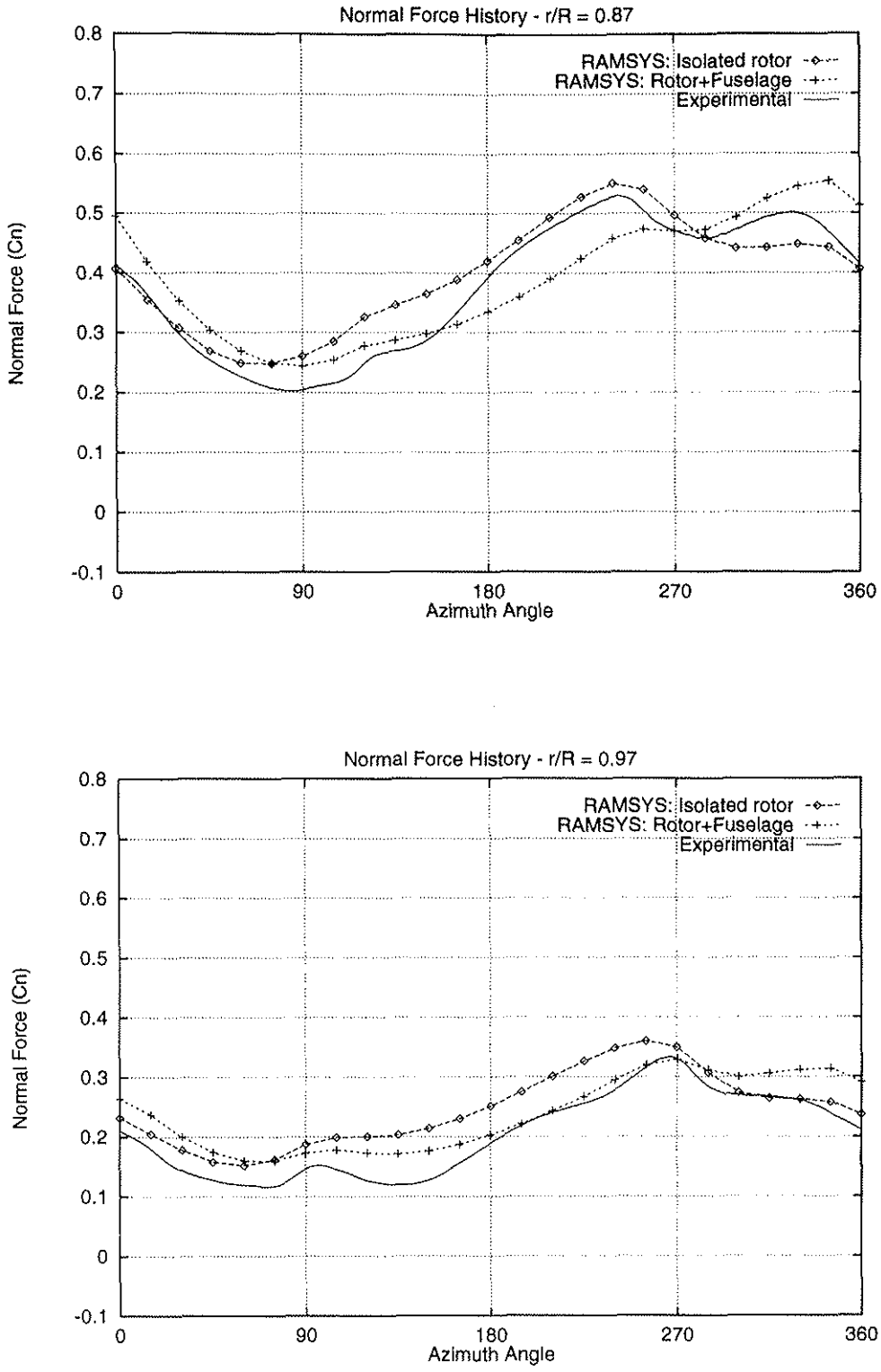

Fig 8 : Normal force time history at two radial stations ($r/R = 0.87, 0.97$)

(DPt 508 : Low-speed 12°-climb, $\mu = 0.15, C_T = 0.00454, M_H = 0.645$)

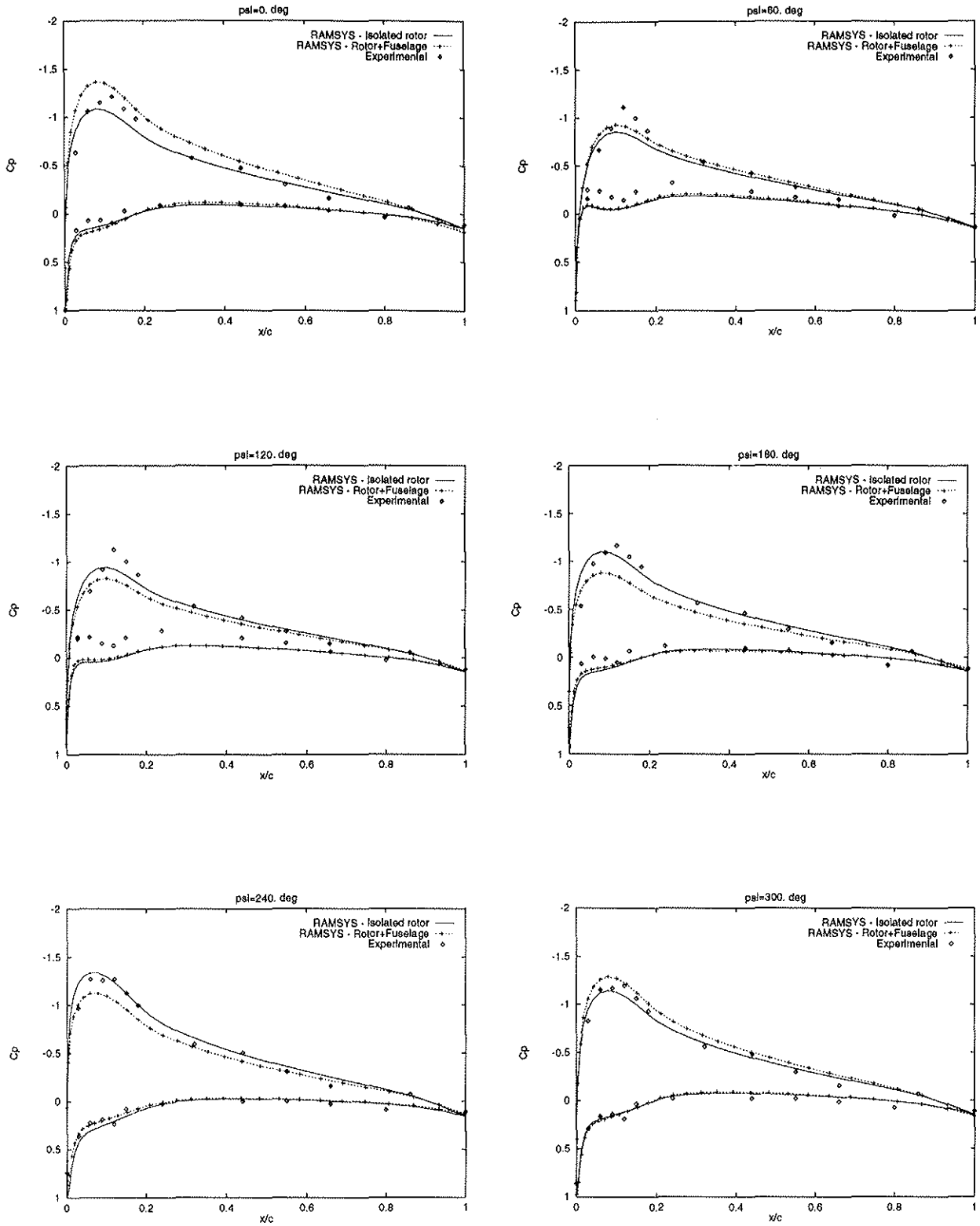

Fig 9 : Chordwise pressure distribution at a single radial station ($r/R = 0.87$) for six azimuthal positions ($\Psi = 0° - 300°$).

(DPt 508 : Low-speed 12°-climb, $\mu = 0.15, C_T = 0.00454, M_H = 0.645$)